

A Real-Time Weather-Adaptive 3DVAR Analysis System for Severe Weather Detections and Warnings

JIDONG GAO,* TRAVIS M. SMITH,⁺ DAVID J. STENSRUD,* CHENGHAO FU,[#] KRISTIN CALHOUN,⁺
KEVIN L. MANROSS,⁺ JEFFREY BROGDEN,⁺ VALLIAPPA LAKSHMANAN,⁺ YUNHENG WANG,[@]
KEVIN W. THOMAS,[@] KEITH BREWSTER,[@] AND MING XUE[@]

* NOAA/National Severe Storms Laboratory, Norman, Oklahoma

⁺ NOAA/National Severe Storms Laboratory, and Cooperate Institute for Mesoscale Meteorological Studies, Norman, Oklahoma

[#] Cooperate Institute for Mesoscale Meteorological Studies, Norman, Oklahoma, and Hunan Meteorological Bureau, Changsa, Hunan, China

[@] Center for Analysis and Prediction of Storms, University of Oklahoma, Norman, Oklahoma

(Manuscript received 17 September 2012, in final form 4 February 2013)

ABSTRACT

A real-time, weather-adaptive three-dimensional variational data assimilation (3DVAR) system has been adapted for the NOAA Warn-on-Forecast (WoF) project to incorporate all available radar observations within a moveable analysis domain. The key features of the system include 1) incorporating radar observations from multiple Weather Surveillance Radars-1988 Doppler (WSR-88Ds) with NCEP forecast products as a background state, 2) the ability to automatically detect and analyze severe local hazardous weather events at 1-km horizontal resolution every 5 min in real time based on the current weather situation, and 3) the identification of strong circulation patterns embedded in thunderstorms. Although still in the early development stage, the system performed very well within the NOAA's Hazardous Weather Testbed (HWT) Experimental Warning Program during preliminary testing in spring 2010 when many severe weather events were successfully detected and analyzed. This study represents a first step in the assessment of this type of 3DVAR analysis for use in severe weather warnings. The eventual goal of this real-time 3DVAR system is to help meteorologists better track severe weather events and eventually provide better warning information to the public, ultimately saving lives and reducing property damage.

1. Introduction

Proper early identification of a supercell thunderstorm, or a supercell embedded in a cluster of storms, is critical to the issuance of public warnings for severe weather. Several studies by Burgess (1976), Burgess and Lemon (1991), and Bunkers et al. (2006, 2009) found the determination of whether a thunderstorm is a supercell thunderstorm is very important to accurate and timely severe weather warning operations. These studies also revealed that over 90% of supercells are severe (i.e., produce tornadoes, large hail, or severe surface winds).

One of the defining characteristics of a supercell is the existence of a midlevel mesocyclone (Lemon and

Doswell 1979). A mesocyclone was originally defined as the Doppler radar velocity signature of a storm-scale (2–10-km diameter) vortex (Burgess 1976), which corresponds to the rotating updraft–downdraft couplet of a supercell thunderstorm. Mesocyclones in the United States are typically cyclonic and also may contain the more intense tornado vortex. In the last 20 years, several criteria have been established for mesocyclone recognition based on a wealth of Doppler radar observations, especially after the deployment of the Weather Surveillance Radar-1988 (WSR-88D) network (Burgess 1976; Burgess et al. 1982, Burgess and Lemon 1991; Burgess and Doswell 1993; Stumpf et al. 1998). Based on these criteria and other conceptual models (e.g., Lemon and Doswell 1979), a mesocyclone detection algorithm (MDA) was developed to help meet the needs of the meteorologists making a warning decision (Stumpf et al. 1998). Although this approach has met with success, some of the hallmark characteristics of supercells, such as the

Corresponding author address: Jidong Gao, NOAA/National Severe Storm Laboratory, 120 David L. Boren Blvd., Norman, OK 73072.

E-mail: jidong.gao@noaa.gov

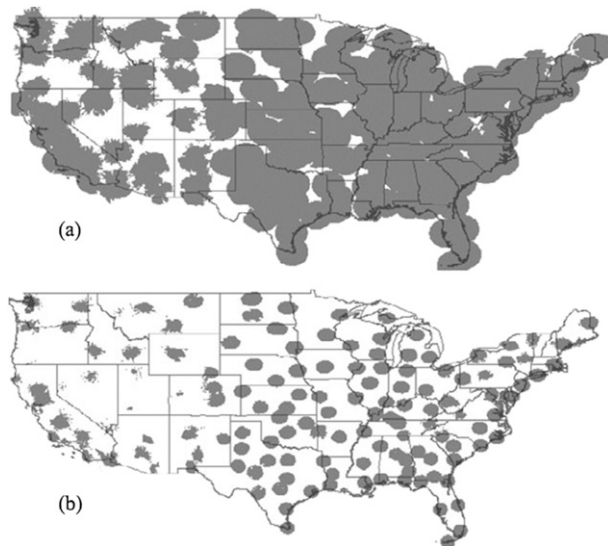


FIG. 1. Coverage of the WSR-88D network at height(s) of (a) 3 and (b) 1 km AGL. These plots are the center of the beam at 0.5° elevation (NEXRAD lowest allowed tilt) (McLaughlin et al. 2009).

depth and persistence of the circulation, the strength of a single updraft core, and the maximum vertical vorticity magnitude, are very difficult to identify with the MDA based upon single-radar observations alone.

Although the low-level (0–1 km AGL) coverage provided by the current WSR-88D network rarely overlaps within the continental United States (Fig. 1b), the mid-level (3–6 km AGL) coverage across the eastern two-thirds of the country is much more complete (Fig. 1a). Thus, observations from multiple WSR-88Ds can be combined to provide an improved three-dimensional wind analysis of storm structure. This type of multiradar approach has already proven useful for improved quantitative precipitation estimation (QPE) and severe weather detection using radar reflectivity observations, as demonstrated by both the National Mosaic and Multi-sensor QPE (NMQ) system (Zhang et al. 2011) and the Warning Decision Support System—Integrated Information (WDSS-II; Lakshmanan et al. 2007b). These systems provide three-dimensional radar reflectivity and azimuthal shear analyses at 1-km resolution every 2.5 min (Lakshmanan et al. 2006). The development of a single high quality analysis that includes observations from multiple sources can help overcome several limitations. First, using multiple observations of the same feature improves the analyses as errors decrease with aggregation. Second, the use of multiple radars can help fill in data voids, such as those below the lowest and above the highest radar scanning angle. Third, while forecasters make their warning decisions based on the best information available, the escalating data flow rates from new

sensors and applications, combined with workload and timeliness requirements, may limit forecasters' ability to effectively use all available information. This situation can be ameliorated by fast data assimilation methods that merge all available information together as quickly as possible for human decision makers.

In this study, we investigate the possibility of identifying mesocyclones by merging all available information from WSR-88D radars together using the Advanced Regional Prediction System (ARPS; Xue et al. 2000, 2001) three-dimensional variational data assimilation system (3DVAR; Gao et al. 2004). The system produces physically consistent high-resolution analyses based on multiple data sources including observations from several nearby WSR-88Ds and operational model forecasts. While the ARPS 3DVAR was originally developed to initialize storm-scale numerical weather prediction (NWP) models, it may also have value in producing accurate real-time wind analyses for use in severe weather warning operations. Not only does the analysis system have the potential to make better use of observations from the WSR-88D network, it can blend in information from operational model forecast products and conventional observational platforms to produce three-dimensional wind analyses valid both inside and outside the storm. Although still in the early development stage, results from initial experiments show that the system performed very well during the spring of 2010 while undergoing testing and evaluation within the Hazardous Weather Testbed (HWT), where many severe weather events were successfully detected and analyzed.

The rest of this paper is organized as follows. Section 2 provides an overview of the 3DVAR data assimilation (DA) system. The data and NWP products used and the analysis procedure description will be presented in section 3. Some preliminary experiment results are reported and assessed in section 4. We conclude in section 4 with a summary and outlook for future work.

2. The ARPS 3DVAR system

The ARPS 3DVAR system was designed and developed especially for radar data assimilation at the convective scale (Gao et al. 1999, 2002, 2004; Xue et al. 2003; Hu et al. 2006a,b; Stensrud and Gao 2010; Ge et al. 2010, 2012). It applies weak constraints that are suitable for convective storms in a different manner than is done with 3DVAR systems developed for large-scale applications. A 3DVAR system starts from a first guess, or background, that is often provided by a forecast model and adjusts the first-guess fields as observations are assimilated. The resulting analysis is a blend of the first guess and the observations. The process is influenced by

assumed constraints and is determined by minimizing a cost function using numerical techniques.

Following Gao et al. (2004), the standard cost function J of 3DVAR can be written as

$$J(\mathbf{x}) = \frac{1}{2}(\mathbf{x} - \mathbf{x}^b)^T \mathbf{B}^{-1}(\mathbf{x} - \mathbf{x}^b) + \frac{1}{2}[H(\mathbf{x}) - \mathbf{y}^o]^T \mathbf{R}^{-1}[H(\mathbf{x}) - \mathbf{y}^o] + J_c(\mathbf{x}). \quad (1)$$

The analysis vector \mathbf{x} contains the three wind components (u , v , and w), potential temperature (θ), pressure (p), and water vapor mixing ratio (q_v), while the cost function equation includes three terms. The first term is the background term, which measures the departure of the analysis vector \mathbf{x} from the background \mathbf{x}^b weighted by the inverse of the background error covariance matrix \mathbf{B} . The background is provided by a numerical model analysis or forecast interpolated in space and time to the 3DVAR domain. The second term is the observation term, which measures the departure of the 3DVAR analysis vector \mathbf{x} from the observation vector \mathbf{y}^o where $H(\mathbf{x})$ is the forward operator that converts from the model variables to the observation. This second term is weighted by the inverse of observation error covariance matrix \mathbf{R} that includes both instrument and representativeness errors. It is usually assumed diagonal, and its diagonal elements are specified according to the estimated observation errors. The third term, $J_c(\mathbf{x})$, represents the dynamic or equation constraints, which are very important for this convective-scale 3DVAR system. All the above three terms are used in this study and are briefly discussed below.

In previous variational Doppler wind analyses (Gao et al. 1999, 2004), the background term is used to provide information on the storm environment. This background information can be from a previous NWP model forecast, a nearby sounding, or a wind profile from another Doppler radar analysis program, such as the velocity azimuth display (VAD) method (Browning and Wexler 1968). In this study, the National Centers for Environmental Prediction’s (NCEP) mesoscale NWP model—the North American Mesoscale model (NAM; Janjić et al. 2003)—is used to produce the background field for the analysis to utilize data from all available sources. While Gao et al. (1999) show that storm analyses are not very sensitive to the background field, the use of a background field allows for the inclusion of environmental information in the analysis. Forecasters are then able to display storm and environmental conditions from a single, unified, dynamically consistent three-dimensional analysis and avoid the difficulties and inconsistencies that can arise when only irregular radar data with many holes and inner boundaries are used.

For the second term, the observation vector \mathbf{y}^o includes WSR-88D radial velocity data only. The radar forward observation operator for radial velocity is written following Doviak and Zrnić (1993) as

$$v_r = \frac{dh}{dr} w + \frac{ds}{dr} (u \sin \phi + v \cos \phi), \quad (2)$$

where v_r is the projected radial velocity, r is the slant range (ray path distance), h is the height above the curving earth’s surface, s is the distance along the earth’s surface, and ϕ is the radar azimuth angle. When WSR-88D radial velocity only is used, the observation error variance is usually set to be between 1 and 2 m s⁻¹, which is typical of radar instrumental error (Doviak et al. 1976; Miller and Sun 2003); we chose the former in this study. The second term in (1) is simplified to

$$J_o(\mathbf{x}) = \frac{1}{2}[H(v_r) - v_r^{\text{ob}}]^2. \quad (3)$$

The analysis is projected into the observation space using the forward operator defined by (2), with a trilinear interpolation operator used to interpolate from model grid points to radar observation locations. However, different from the Weather Research and Forecasting (WRF) model’s 3DVAR scheme (Barker et al. 2004), which was designed mainly for synoptic and mesoscale data assimilation, the ARPS 3DVAR approach uses multiple analysis passes that have different spatial influence scales. The use of multiple passes is found to be advantageous for analyzing convective storms (Hu et al. 2006b; Gao et al. 2009; Schenkman et al. 2011). The quality control within the ARPS 3DVAR also includes buddy checking, velocity dealiasing for radar data, and the removal of anomalous propagation returns.

In the ARPS 3DVAR, cross correlations among state variables are not included in the background error covariance \mathbf{B} ; a certain degree of balance between analysis variables is realized by incorporating weak constraints in the cost function as the $J_c(\mathbf{x})$ term in (1). In this study, a constraint is imposed on the analyzed wind components based on the anelastic mass continuity equation, such that

$$J_C = \frac{1}{2} \lambda_c (\partial \bar{p} u / \partial x + \partial \bar{p} v / \partial y + \partial \bar{p} w / \partial z)^2, \quad (4)$$

where \bar{p} is the mean air density at a given horizontal level and the weighting coefficient λ_c , controls the relative importance of this penalty term in the cost function. The value of $\lambda_c = 5.0 \times 10^{-4}$ is used for the current application. This value determines the relative importance of the mass continuity equation constraint and its

optimal value is determined through many numerical experiments in a trial-and-error fashion (Gao et al. 1999; Sun and Crook 2001). Gao et al. (1999, 2004) found that this constraint is effective in producing suitable analyses of vertical velocity, as it builds up the relationship among the three wind components. As pointed out in Gao et al. (1999), using the mass continuity equation as a weak instead of a strong constraint avoids the error accumulation associated with the explicit vertical integration of the mass continuity equation, as is often used in conventional dual-Doppler wind synthesis schemes. Thus, thunderstorm updrafts can be more accurately analyzed and the analysis is less sensitive to the lower and upper boundary conditions than occur when a mass continuity equation is used as a strong constraint. The use of the weak mass continuity constraint links the three components of the wind field by the 3DVAR method in response to the assimilation of the radial velocity observations.

To effectively precondition the minimization problem, we follow Courtier et al. (1994) and Courtier (1997) and define an alternative control variable \mathbf{v} , such that $\mathbf{B}^{1/2}\mathbf{v} = (\mathbf{x} - \mathbf{x}_b)$. This allows the cost function to be changed into an incremental form, such that

$$J_{\text{inc}}(\mathbf{v}) = \frac{1}{2}\mathbf{v}^T\mathbf{v} + \frac{1}{2}(\mathbf{H}\mathbf{C}\mathbf{v} - \mathbf{d})^T\mathbf{R}^{-1}(\mathbf{H}\mathbf{C}\mathbf{v} - \mathbf{d}) + J_c(\mathbf{v}), \quad (5)$$

where \mathbf{H} is the linearized version of H and $\mathbf{d} \equiv \mathbf{y}^o - H(\mathbf{x}^b)$. The gradient and Hessian of J_{inc} can also be derived, with the former obtained by differentiating (5) with respect to \mathbf{v} , yielding

$$\nabla J_{\text{inc}} = (\mathbf{I} + \mathbf{C}^T\mathbf{H}^T\mathbf{R}^{-1}\mathbf{H}\mathbf{C})\mathbf{v} - \mathbf{C}^T\mathbf{H}^T\mathbf{R}^{-1}\mathbf{d} + \nabla J_c(\mathbf{v}), \quad (6)$$

where \mathbf{I} is the identity matrix. The Hessian then follows as

$$\nabla^2 J_{\text{inc}} = \mathbf{I} + \mathbf{C}^T\mathbf{H}^T\mathbf{R}^{-1}\mathbf{H}\mathbf{C} + \nabla^2 J_c(\mathbf{v}). \quad (7)$$

From (7), it is clear that the preconditioning prevents the smallest eigenvalue from becoming close to zero. This potentially could improve the convergence of minimization algorithms and allows the variational problem to be solved more efficiently.

The matrix \mathbf{C} defined in (5) can be broken down as

$$\mathbf{C} = \mathbf{D}\mathbf{F}\mathbf{L}, \quad (8)$$

where \mathbf{D} is a diagonal matrix consisting of the standard deviation of background errors and \mathbf{L} is a scaling factor.

The matrix \mathbf{F} is the square root of a matrix with diagonal elements equal to one and off diagonal elements equal to the background error correlation coefficients. However, the matrix \mathbf{F} is too large to be used directly in the minimization calculations. Instead, it is modeled by a spatial recursive filter (Purser et al. 2003), which in first order is defined by

$$\begin{aligned} Y_i &= \alpha Y_{i-1} + (1 - \alpha)X_i \quad \text{for } i = 1, \dots, n \\ Z_i &= \alpha Z_{i+1} + (1 - \alpha)Y_i \quad \text{for } i = n, \dots, 1, \end{aligned} \quad (9)$$

where X_i is the initial value at grid point i , Y_i is the value after filtering for $i = 1$ to n , Z_i is the initial value after one pass of the filter in each direction, and α is the filter coefficient given by the following formulation (Lorenz 1992):

$$\begin{aligned} \alpha &= 1 + E - \sqrt{E(E + 2)} \\ E &= 2N\Delta^2/4L^2, \end{aligned} \quad (10)$$

where L is the horizontal correlation scale, Δ is the horizontal grid spacing, and N is the number of filter passes to be applied. This is a first-order recursive filter, applied in both directions to ensure zero phase change. Multipass filters (N greater than unity) are built up by repeated application of (9) and (10). In this study, two passes of the recursive filter are used ($N = 2$). The first pass uses $L = 12$ km and is followed by a second pass using $L = 4$ km to provide an improved representation of the convective-scale features within the analysis. Xie et al. (2005, 2011) proved theoretically that the multiple-passes approach with a recursive filter is superior to the conventional single-pass 3DVAR method. Zhang et al. (2009) designed a successive localization approach as part of a similar strategy for an ensemble Kalman filter technique to assimilate dense radar observations that contain information about the state of the atmosphere at a wide range of scales in a hurricane-related study.

As discussed earlier, reflectivity data are not used directly in the ARPS 3DVAR data assimilation system. Reflectivity observations instead are interpolated to the analysis grid from the observed radar reflectivity using the method developed in Zhang et al. (2005). For real-time NWP applications, the ARPS 3DVAR has often been used together with a cloud analysis scheme to analyze the hydrometeor variables and to adjust in-cloud temperature and moisture fields (Brewster et al. 2005; Hu et al. 2006a,b). The cloud analysis is not necessary for the current application because our focus is on the internal circulation structures, including updrafts within thunderstorms.

Gao and Stensrud (2012) present a method for directly assimilating reflectivity using (1) in a convective-scale,

cycled 3DVAR simulation with hydrometeor classification in a reflectivity observation operator. In this approach, a modified forward operator for radar reflectivity is developed that uses a background temperature field from a numerical weather prediction model for hydrometeor classification. The analysis vector \mathbf{x} in (1) is expanded to include rainwater, snow, and hail. A diagnostic pressure equation derived from the modified ARPS momentum equations also can be used as an additional weak constraint in the 3DVAR scheme, providing a coupling between the wind components and the thermodynamic variables (Ge et al. 2012). Numerical experiments in Ge et al. (2012) show that the use of new equation constraints can speed up the spinup of precipitation during the intermittent data assimilation process and improve the follow-on forecasts in terms of the general evolution of storm cells and mesocyclone rotation. However, in the current study, for simplicity and computational speed, only the mass continuity constraint is included and only radar radial velocity data are assimilated. The more advanced features of the 3DVAR program will be integrated into our real-time applications in the future.

3. Input data and procedure description

The main concern in setting up the 3DVAR model to run in real time for testing and evaluation within the HWT is latency—the time delay between when the WSR-88D observations arrive and the 3DVAR analysis is available. If the time delay is too long, then forecasters will largely ignore the analyses as thunderstorms evolve quickly. However, a second concern is the analysis domain size. The challenge is to choose domains large enough to contain the principal features of meteorological interest while maintaining an efficient computational advantage so that the analyses can be produced fast enough to be of use in operations. Thus, for the currently available computing power, the analysis domain size is limited to allow for a time delay of 4 min or less. With continued improvements in computational power and code efficiency, this time delay could be decreased significantly. The domain selected has 200×200 horizontal grid points with a 1-km grid spacing. In the vertical direction, 31 terrain-following vertical layers are used, with nonlinear stretching via a hyperbolic tangent function, thus yielding an average vertical grid spacing of 400 m. To allow for forecasters within the HWT to evaluate the 3DVAR products in various severe weather scenarios, four separate sets of $200 \text{ km} \times 200 \text{ km}$ 3DVAR analyses within four different domains are provided at any given time and updated with new observations every 5 min.

A two-dimensional (2D) composite reflectivity product covering the 48 contiguous United States from the WDSS-II real-time system (Lakshmanan et al. 2007b) at the National Severe Storm Laboratory (NSSL) is used to identify the four locations (latitude, longitude) at risk for severe storms. The quality control attempts to remove nonmeteorological echoes due to radar artifacts, test patterns, anomalous propagation (Lakshmanan et al. 2007a), biological targets (Lakshmanan et al. 2010), and persistent clutter (Lakshmanan et al. 2012). These four locations are chosen based upon where the values of radar reflectivity are the largest from the most current 2D reflectivity product, and are updated every 30 min based upon the most recent 5-min 2D composite reflectivity field. To make sure that the four analysis domains have little overlap, the selection of the second largest value of reflectivity is required to be at least 100 km away from the location of the first largest value of reflectivity; the same requirement is applied successively in the selection of the other two domains, such that all identified locations are at least 100 km from one another. The identified four locations are then used as the centers for the four 3DVAR analysis domains. Because of limitations of computer resources, we want to select locations where severe weather events are most likely to happen. The idea of developing a weather-adaptive numerical model and observation system was discussed in Droegemeier et al. (2005).

Once the analysis domains are selected, the next step is to include the necessary background data. Terrain data are interpolated onto the selected analysis domains. The latest available NCEP operational NAM (Janjic et al. 2003) analysis and forecasts are obtained and interpolated onto the 3DVAR domains using linear interpolation in time and quadratic interpolation in space. The NAM model is a regional mesoscale forecast system based on the WRF common modeling infrastructure, currently running with 12-km horizontal grid spacing and 60 vertical layers. New NAM forecasts are produced every 6 h from 0000, 0600, 1200, and 1800 UTC, with forecast output available every 3 h out to 84 h. The most recent NAM forecast cycle is used to provide the background data for the 3DVAR.

The third step is to determine how many operational WSR-88Ds contain relevant data within each of the four selected domains. To ensure maximum data coverage, a larger domain of $500 \text{ km} \times 500 \text{ km}$ with the same center location is used to determine which WSR-88Ds are needed in the 3DVAR analysis. Observations from the selected WSR-88D locations are then obtained in real time in their raw data format from Integrated Robust Assured Data Services (IRADS) of the University of Oklahoma with a data latency of about 10–20 s from the end of the volume scan. The necessary quality control

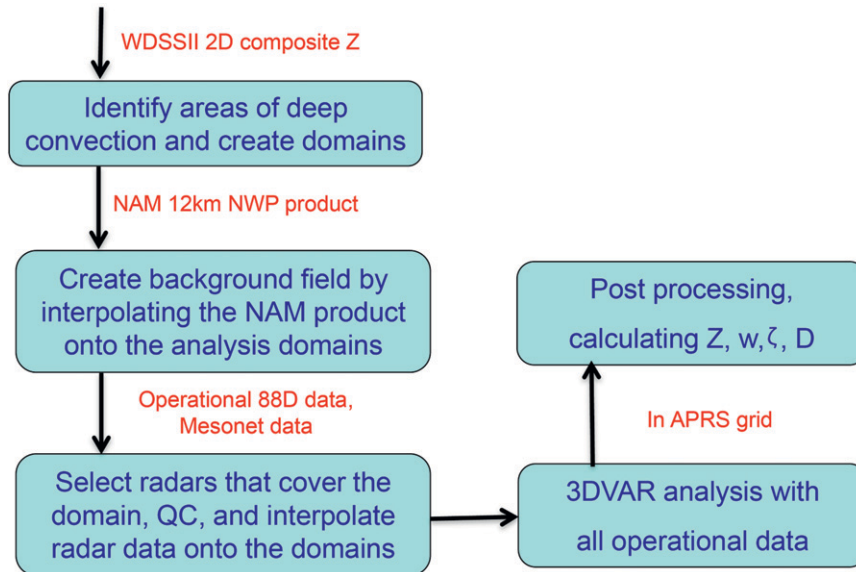


FIG. 2. Flowchart showing the weather-adaptive 3DVAR system.

steps, including velocity dealiasing and ground clutter removal, are performed on the observations from each radar individually. After the quality control is completed, a three-dimensional interpolation scheme with a second-order local polynomial function fitting of the radar data onto the analysis grids is performed (Daley 1992).

The 3DVAR analysis is then completed using both the background field obtained from the NAM and the interpolated and quality-controlled WSR-88D data using a quasi-Newton descent algorithm to solve (1) following Liu and Nocedal (1989). Once the analysis is complete, postprocessing occurs, which includes identifying the positions of supercells, and obtaining two-dimensional composite vertical vorticity and vertical velocity tracks, as well as various other fields from the analyses.

The complete 3DVAR real-time system procedure is shown schematically in Fig. 2 and is performed every 5 min using a local computer with 128 processors (each domain with 32 processors) and Message Passing Interface (MPI) supported computational capacity (Gropp et al. 1999). The MPI implementation of the 3DVAR utilizes a domain-decomposition scheme that is commonly used with NWP models. The analysis domain is evenly divided into patches in both the west–east and south–north directions. The cost function is computed separately over each patch in parallel, and then the summation is collected. The arrays that are used to hold the analysis variables in the computer memory are extended with one extra grid in each horizontal direction for handling the linear interpolations of variables from the model grid space to the observation space. With this implementation the computation order of the cost

function is inevitably changed. Considering the computer representation error for a floating point number, it is impossible to obtain the identical analysis as results from a serial program. The differences, however, are very small and practically insignificant for storm analysis applications. Furthermore, the representation error can be reduced by increasing the number of representation digits (e.g., using double precision floating numbers). One of the difficult parts of the parallelization is designing an efficient parallel algorithm for the recursive filter operations. A simple parallel scheme that advances the recursive filter patch by patch in each horizontal direction is used in the 3DVAR scheme. This scheme achieves a moderate level of parallelization with a simple and straightforward code implementation. Fortunately, the computation of recursive filters only accounts for a small amount of the whole analysis so the impact to the total parallel performance by using such a simple scheme is not significant. On average, each analysis is finished in about 4 min or less and typically three or four radars are included. As an initial application, the focus is on the 3D wind analyses and wind-derived variables, such as vertical velocity and vorticity. In the future, with available enhancements to the 3DVAR and the use of additional nonradar observations, other model variables, such as potential temperature, and humidity and hydrometeor fields, could also be provided.

4. Some preliminary results

The reliability and accuracy of the ARPS 3DVAR system for severe thunderstorm analysis have been

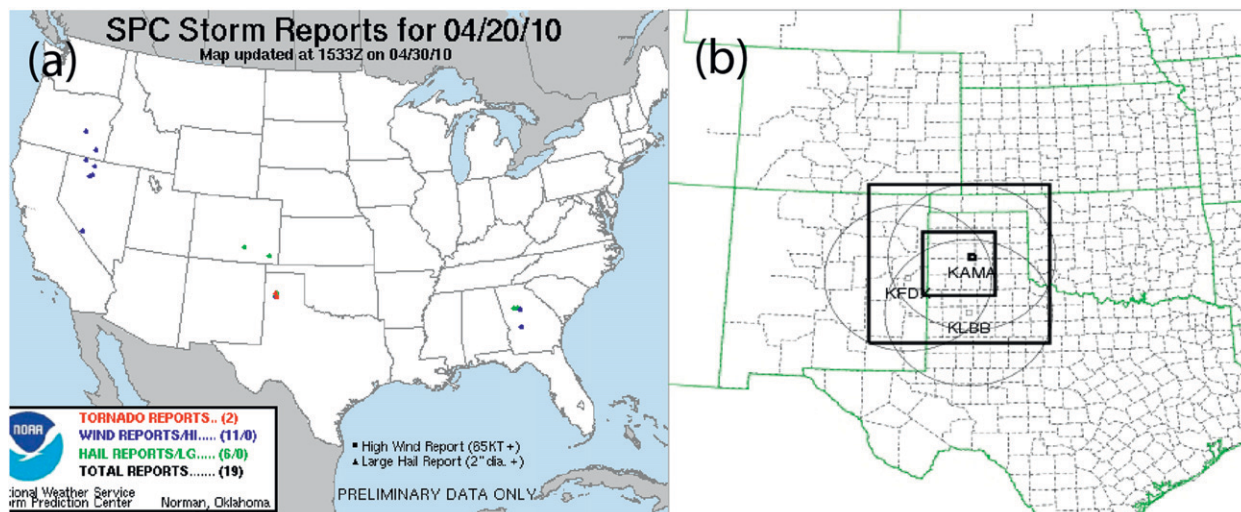


FIG. 3. Texas Panhandle tornadic storm event on 20 Apr 2010. (a) The storm report from SPC and (b) the illustration of the 3DVAR analysis domain. The inner domain of $200 \text{ km} \times 200 \text{ km}$ is used for 3DVAR analysis. The outer domain of $500 \text{ km} \times 500 \text{ km}$ is used to identify WSD-88D radars to be used. WSD-88D radars used are KAMA, KFDX, and KLBB.

illustrated by a number of numerical experiments with both simulated and real data cases (e.g., Gao et al. 1999, 2002, 2004; Hu et al. 2006b; Ge et al. 2010, 2012; Stensrud and Gao 2010; Schenkman et al. 2011; Zhao et al. 2012). Examples of successful applications of the system include real-time low-level wind analyses (Gao et al. 2010) and initializing high-resolution real-time severe weather forecasts (Brewster et al. 2010) using radar data from the Engineering Research Center for Collaborative Adaptive Sensing of the Atmosphere (CASA) IP1 network supported by National Science Foundation (McLaughlin et al. 2009). The system also has been used since 2008 to provide initial conditions for very high-resolution (1–4-km grid spacing) deterministic and ensemble WRF model runs that assimilate WSR-88D radar data over a continental U.S. domain in support of the HWT Experimental Forecast Program (EFP; Xue et al. 2008). The HWT/EFP is focused on the use of computer models of the atmosphere to improve predictions of hazardous and convective weather events from a few hours to a week in advance.

To assess the potential usefulness of the weather-adaptive real-time analysis system based on the ARPS 3DVAR to warning operations, it was informally tested and evaluated by forecasters who participated in another HWT program—the Experimental Warning Program (EWP) in 2010. The 3DVAR system was run intermittently from 15 April to 15 June during the spring of 2010. During this time period, over a dozen severe weather events were successfully and automatically identified and analyzed by the 3DVAR system. For all these cases, the storm automatic positioning system performed very well. In general, strong circulation patterns and

vertical velocities associated with severe weather events were all successfully analyzed and identified. These analyses not only collocated quite well with synthesized reflectivity fields from multiple radars, but also agreed well with archived Storm Prediction Center (SPC) storm reports, which provide data about severe weather events including tornadoes, hailstorms, and strong wind events. The performance of the system, including the automatic storm positioning capability, on four tornadic supercell cases observed during this time period is examined below.

a. The 20 April tornadic supercell storm in the Texas Panhandle

The first case is a tornadic supercell that occurred on 20–21 April 2010 over the Texas Panhandle. A single supercell was observed over a 4-h period from 2200 UTC 20 April to 0200 UTC 21 April. At least two tornadoes, large hail, and strong winds were reported during the lifetime of the storm (Fig. 3a). Radial velocity observations from several nearby WSR-88Ds, including those at Amarillo (KAMA) and Lubbock (KLBB) in Texas, and Cannon Air Force Base (AFB), New Mexico (KFDX), were incorporated into the 3DVAR analyses (Fig. 3b).

The supercell storm started near the New Mexico–Texas state line. During the first 2 h, the circulation in the storm was not very strong, but the mesocyclone within the supercell intensified just prior to 0000 UTC 21 April. Near 0004 UTC the first weak tornado was reported, after which the storm continued to develop and grew in intensity. The automated floating 3DVAR domain followed the evolution of this storm very closely. The analyzed horizontal winds, vertical vorticity, and the

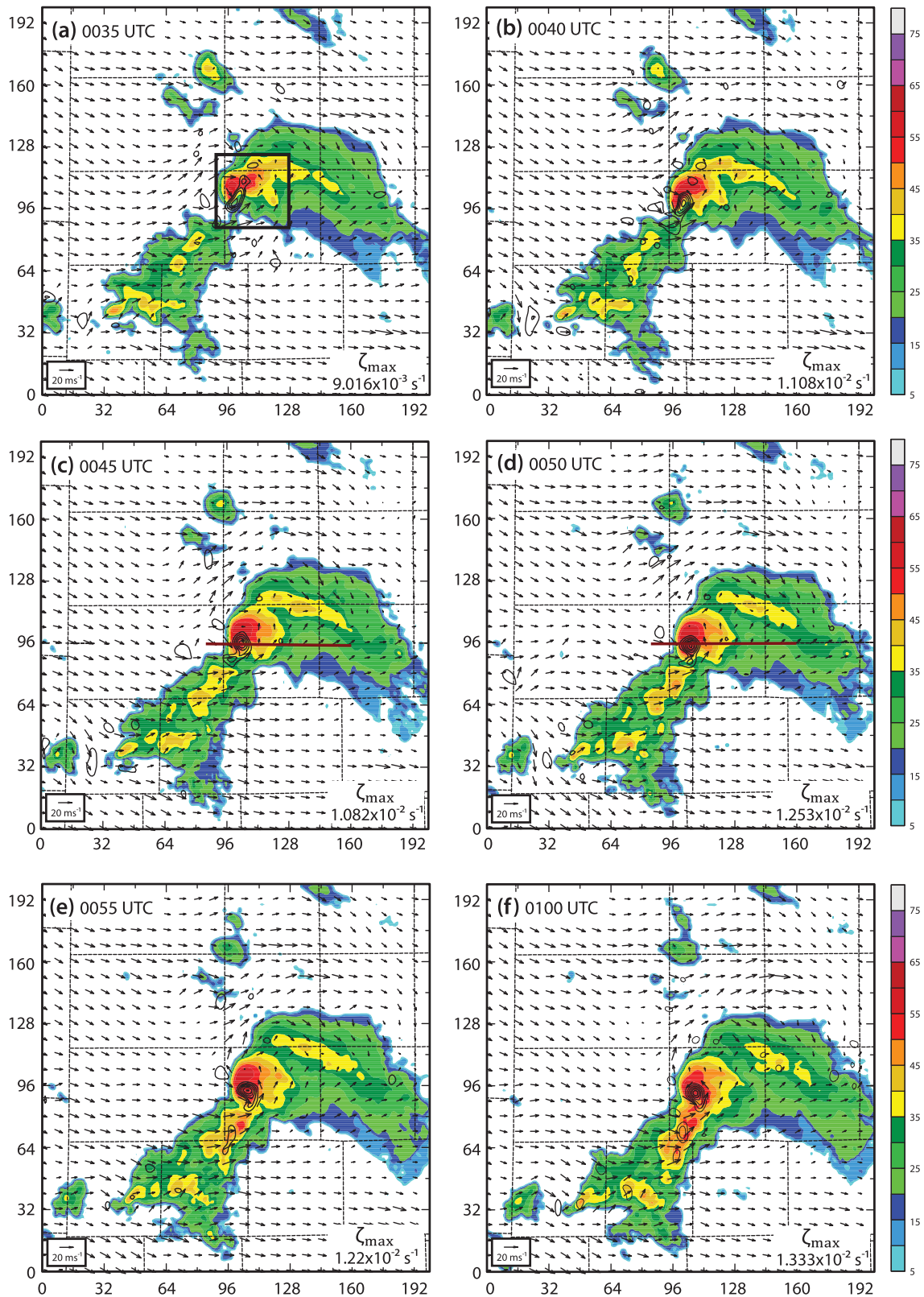


FIG. 4. The synthesized reflectivity (color shaded, dBZ), horizontal wind fields (vectors, m s^{-1}), and vertical vorticity (contour interval is $2 \times 10^{-3} \text{ s}^{-1}$) at 3 km AGL using data from WSR-88D radars shown in Fig. 3b, at (a) 0035, (b) 0040, (c) 0045, (d) 0050, (e) 0055, and (f) 0100 UTC 20–21 Apr 2010 near Umbarger, TX. Maroon line denotes location of cross sections in Fig. 5. Black box in (a) is the zoom-in area for Fig. 6.

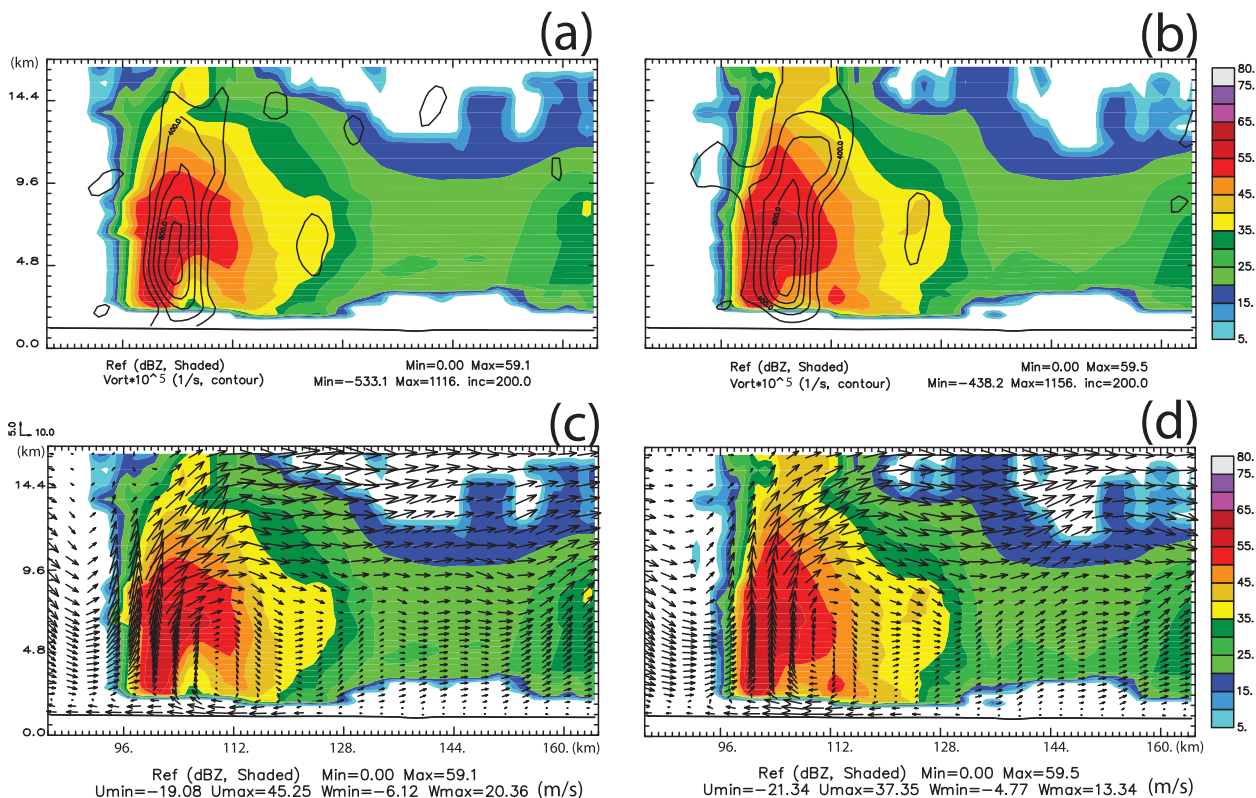


FIG. 5. (a),(b) Vertical vorticity (black contours), (c),(d) wind vectors, and (a)–(d) reflectivity (color shaded) along a vertical slice indicated in Fig. 4, at (left) 0045 and (right) 0050 UTC 20 Apr 2010 near Umbarger. Between these two time levels, a tornado touched down.

interpolated radar reflectivity at 3 km AGL suggest that the storm was at peak intensity from 0030 to 0100 UTC 21 April (Fig. 4). During this half-hour period, a strong closed circulation pattern was evident at 3 km AGL with maximum vertical vorticity above 0.01 s^{-1} at almost all times. The strong mesocyclone (indicated by the vertical vorticity) was approximately collocated with the reflectivity core, and extended through about 10 km in height at both 0045 and 0050 UTC (Fig. 5). A weak-echo region (WER) was also evident near the center of the storm below 4 km AGL (Figs. 5a and 5c) and low-level storm inflow was clearly shown. A second tornado touched down near 0047 UTC (SPC storm reports; Fig. 3a). A gradual occlusion of the hook echo and wind fields occurred from 0035 to 0100 UTC (Figs. 6a–f), and it appears that the second tornado touched down in the middle of this occlusion process (from 0045 to 0055 UTC). During this period, this storm also produced large hail according to SPC storm reports (Fig. 3a).

b. The 25 May tornadic supercell storm in west Kansas

The second case is a tornadic supercell that took place on 25 May 2010 near Gove, Kansas. Two supercells

developed over a 3-h period and produced over a dozen tornadoes (Fig. 7a). Several nearby WSR-88Ds, including Goodland, Kansas (KGLD); Hastings, Nebraska (KUEX); Vance AFB, Oklahoma (KVNK); and Dodge City, Kansas (KDDC), were automatically identified by the 3DVAR domain selection system, and observations from these radars were used in the 3DVAR analyses (Fig. 7b).

The 3DVAR system captured the evolution of two supercell storms from 0100 to 0130 UTC 26 May. During this half-hour period, a hook echo for the strongest storm cell in the center of the analysis domain is seen in the reflectivity field at 3 km AGL (Figs. 8a–f). This cell, along with the weaker, rotating-storm cell to the southwest, moved slowly from west to east across the center of the analysis domain. The wind analyses at 3 km AGL indicate a very strong midlevel cyclonic circulation with vertical vorticity $>0.01 \text{ s}^{-1}$ within the central, stronger storm that persisted and was collocated with the reflectivity hook echo throughout the period. The mesocyclone maintained its strength with a vertical extent consistently about 10 km deep AGL (not shown). The storm produced large hail throughout the analysis period and tornadoes were reported at 0106, 0114, and

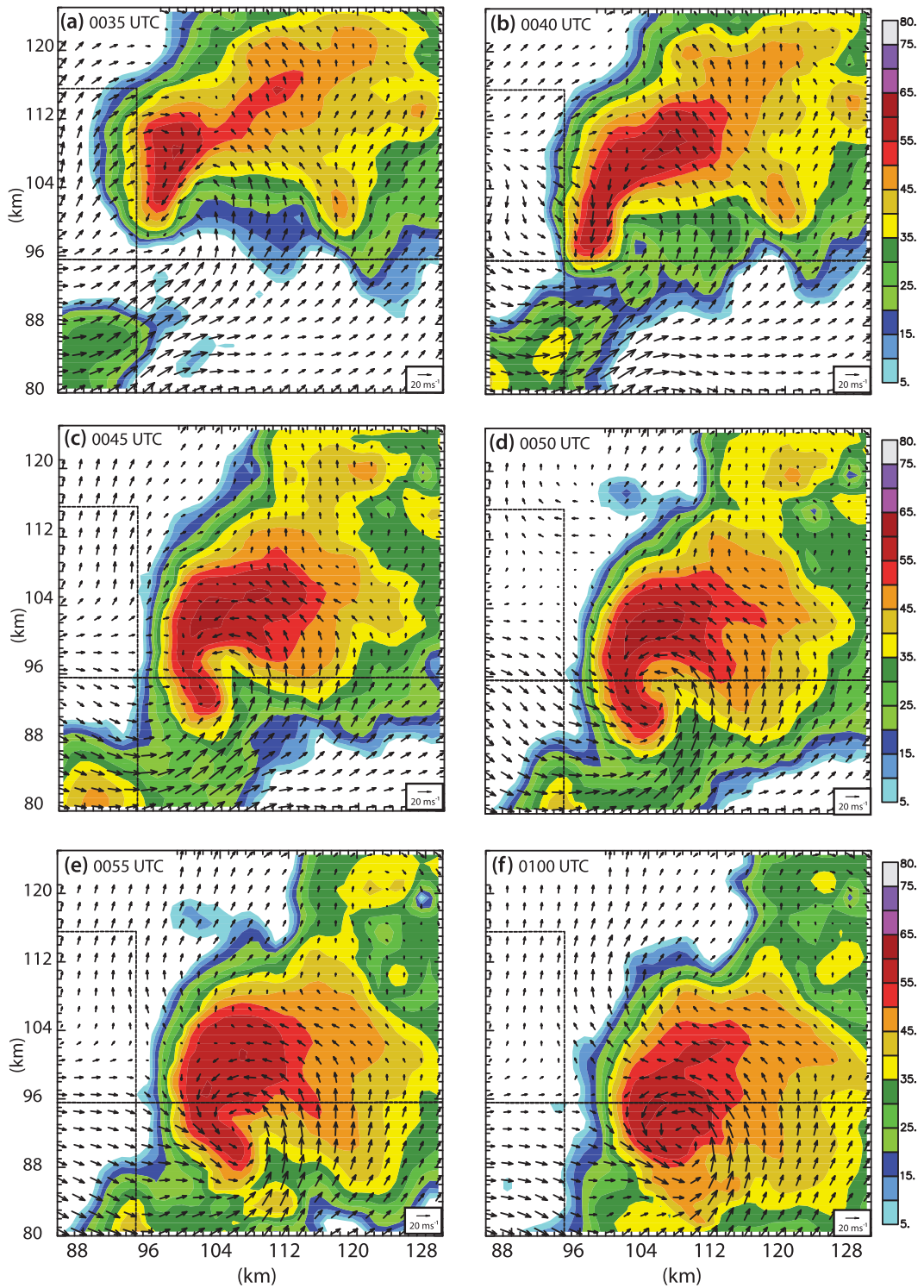


FIG. 6. The synthesized reflectivity (color shaded, dBZ) and horizontal wind fields (vectors, m s^{-1}), at 1.5 km AGL zoomed in from the box in Fig. 4a, at (a) 0035, (b) 0040, (c) 0045, (d) 0050, (e) 0055, and (f) 0100 UTC 20–21 Apr 2010 near Umbarger.

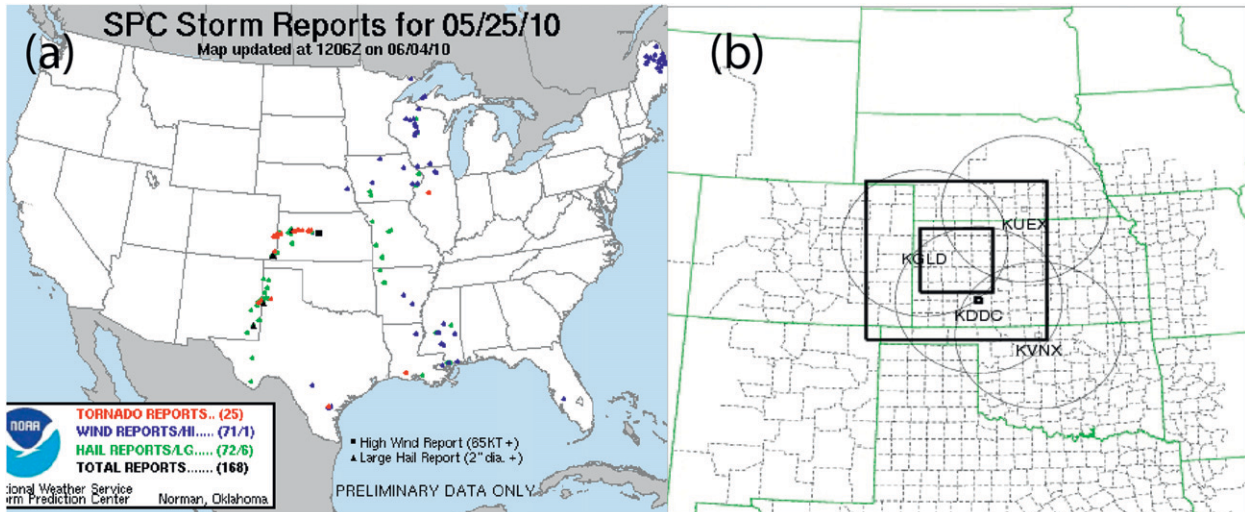


FIG. 7. As in Fig. 3, but for 25 May 2010 KS tornadic storm event. WSD-88D radars used are KGLD, KUEX, KDDC, and KVNX.

0128 UTC in Gove, Kansas (SPC storm reports; Fig. 7a); the timing of the events agrees quite well with the presence of the strong mesocyclone embedded in this supercell.

c. The 31 May tornadic supercell storm in Colorado and the Oklahoma panhandle

The third case examined is a tornadic supercell event that occurred along the Colorado and Oklahoma border on 1 June 2010 (Fig. 9a). Four nearby WSR-88Ds, including KAMA; Pueblo, Colorado (KPUX); KGLD; and KDDC, were selected by the 3DVAR system and used in the analyses (Fig. 9b). However, all four of these WSR-88Ds are located farther away from the storm center than seen in previous cases (Fig. 9). As indicated in Fig. 1, the midlevel coverage from the WSR-88D network is not as complete across the Oklahoma panhandle and the low-level coverage over the domain is nonexistent. However, important storm structures in the middle and upper levels were still detected within the 3DVAR analyses (Figs. 10 and 11). A strong midlevel mesocyclone was evident with maximum vertical vorticity greater than 0.01 s^{-1} maintained throughout the 0100–0125 UTC period (Figs. 10a–f). The analysis at 1 km AGL shows no sign of a severe storm, which is expected because there are no radar observations at this low level. Vertical slices through the center of the storm indicate that there were no radar echoes below 2 km AGL, though a strong, narrow mesocyclone is embedded in the reflectivity core above 2 km AGL (Figs. 11a and 11b) and the updraft core matches quite well with the reflectivity observations in the middle and upper parts of the storm (Figs. 11c and 11d). During this time period, several tornadoes were observed near Campo,

Colorado, and reported to last for at least several minutes (Fig. 9a). This case shows that mesocyclones associated with tornadoes can still be detected in a 3DVAR analysis using data from the WSR-88D radar network even when the low-level radar coverage is not very good.

d. The 10 June tornadic supercell storm in Denver, Colorado

The final case is a tornadic supercell event that took place near Denver, Colorado, on 11 June 2010 (Fig. 12a). Observations from four WSR-88D radars, including Denver, Colorado (KFTG); Cheyenne, Wyoming (KCYS); KGLD; and KPUX, were identified and used in the 3DVAR analyses (Fig. 12b). The two supercell storms that produced tornadoes were located in close proximity to KFTG. There were several storm clusters that propagated from west to east within the analysis domain, with the distribution of convective available potential energy (CAPE) generally increasing from west to east (Fig. 13). With strong easterly inflow, both storms were ingesting environmental air with CAPE in excess of 2000 J kg^{-1} , with a tongue of higher CAPE air flowing into the southern storm. This ease of visualization of environmental and storm information overlaid with each other is one benefit of this 3DVAR approach. Two major supercells near the center of the analysis domain moved slowly eastward during the analysis period from 0100 to 0145 UTC. The northern storm produced the first tornado, but weakened by 0130 UTC while propagating to the east. The southern storm cell intensified throughout the period as it moved east and produced three tornadoes at 0010, 0120, and 0146 UTC (Fig. 12a). The mesocyclone within the southern primary reflectivity core was even narrower and more concentrated than is

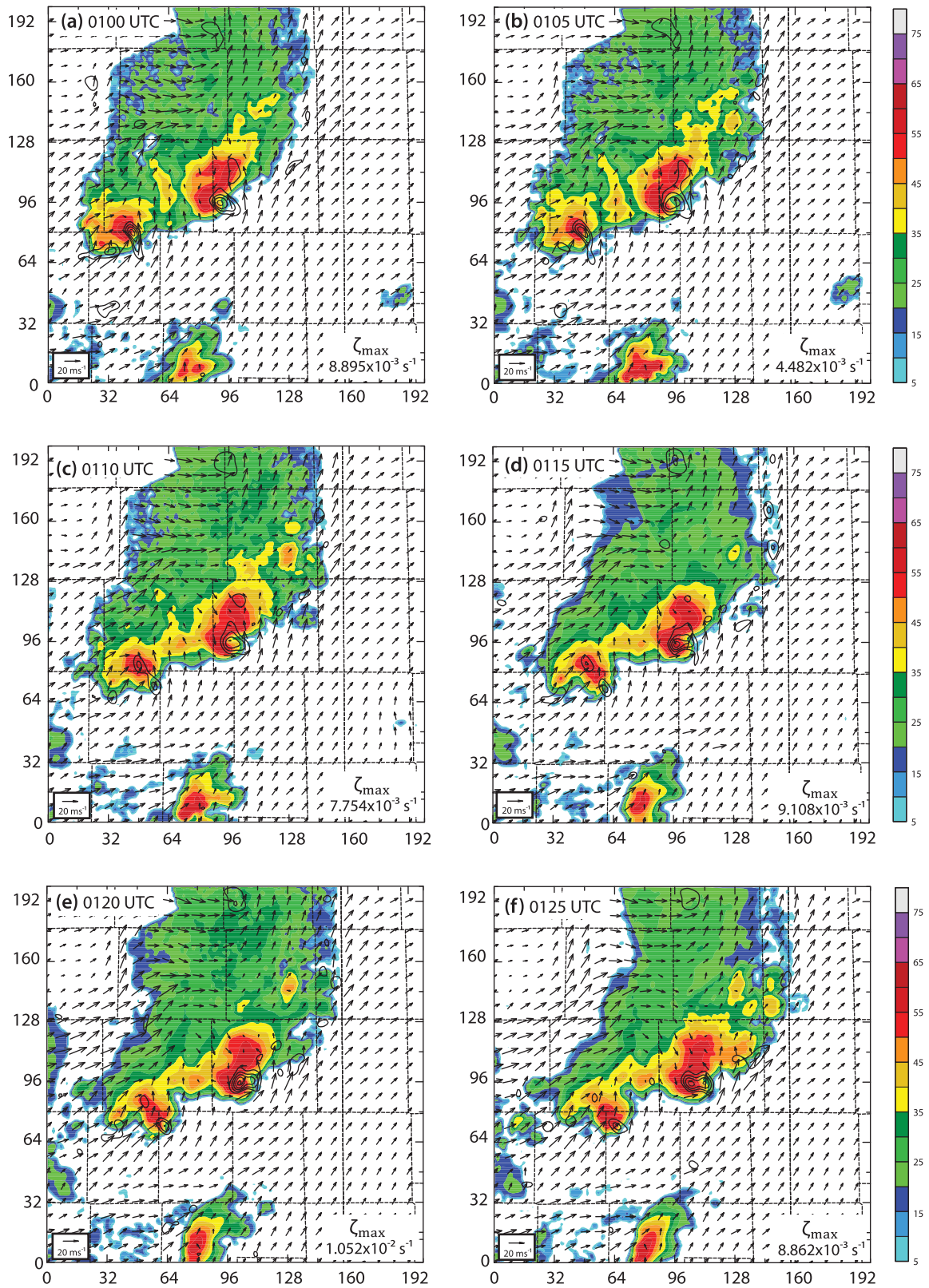


FIG. 8. As in Fig. 4, but for the Gove, KS, tornadic supercell event, using data from radars shown in Fig. 7, at (a) 0100, (b) 0105, (c) 0110, (d) 0115, (e) 0120, and (f) 0125 UTC 26 May 2010.

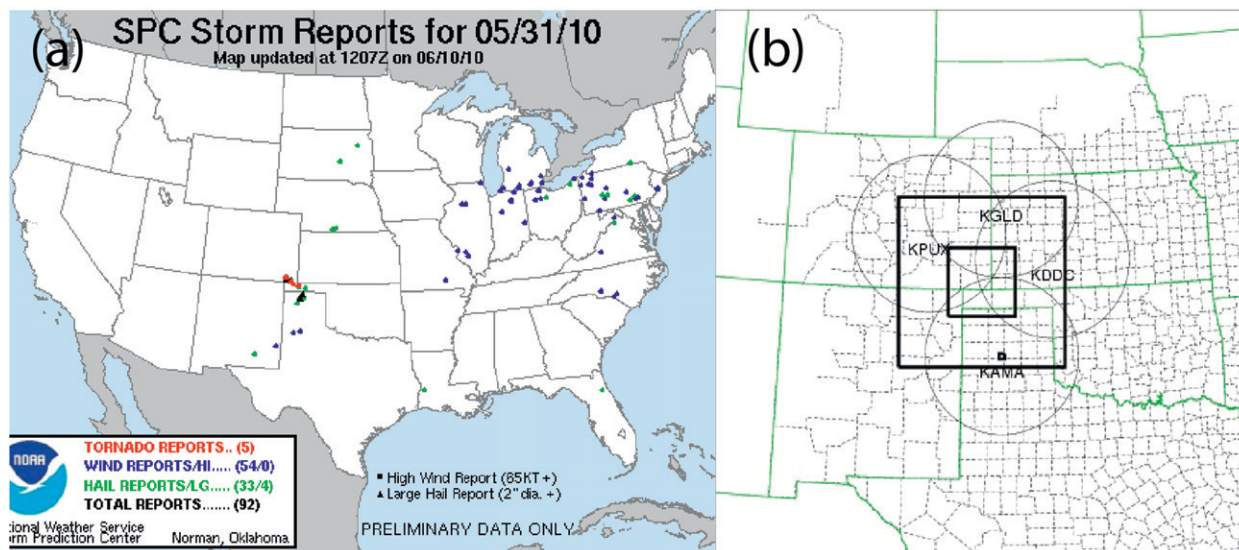


FIG. 9. As in Fig. 3, but for the Campo, CO, tornadic storm event on 31 May 2010. WSD-88D radars used are KGLD, KPUX, KDDC, and KAMA.

seen in the previous cases with a deeper vertical extent of nearly 15 km (Figs. 14a and 14b). Associated with the mesocyclone and reflectivity core, a strong narrow updraft core was also embedded in this southern supercell (Figs. 14c and 14d). A downdraft was also evident on both the upwind and downwind flanks of the supercell's updraft, which agrees with classic supercell conceptual models (Ray and Wagner 1976; Lemon and Doswell 1979). These downdrafts occur outside of the reflectivity region and their strengths may be influenced by the background fields provided by the NAM forecasts subject to mass continuity constraint. A reflectivity overhang and a weak-echo region associated with strong rotational inflow were also captured by the analyses (Fig. 14).

5. Summary and concluding remarks

Doppler radar is a fundamental tool for severe storm monitoring and nowcasting activities. Forecasters examine real-time WSR-88D observations and radar algorithm products, and use their considerable experience and situational awareness to issue severe storm warnings that help protect the public from hazardous weather events. However, there are situations for which even the best forecasters find it challenging to make a quick and sound judgment based on the information from a multitude of sources. To take more complete advantage of the full information content from the current WSR-88D radar network and high-resolution NCEP operational model analysis and forecast products, we developed a weather-adaptive 3DVAR analysis system for severe

weather detection. The focus of this 3DVAR system is the detection of mesocyclones at middle atmospheric levels between 3 and 5 km AGL.

This radar-based analysis system has been adapted from the 3DVAR method originally developed for initializing the ARPS forecast model for storm-scale predictions, and is shown to have the potential to provide improved information for making severe weather warning decisions. Some key features of the system include 1) incorporating radar observations from multiple WSR-88Ds with NCEP forecast products as a background state, 2) the ability to automatically detect and analyze severe local hazardous weather events at 1-km horizontal resolution every 5 min in real time based on the current weather situation, and 3) the identification of strong midlevel circulations embedded in thunderstorms. While designed for real-time testing, the analysis system also can be run offline. This enables, for example, the study of a specific area in greater detail or the investigation of the evolution and lifetime of certain kinds of severe weather not analyzed by this system previously.

The potential usefulness of this system has been demonstrated by examining the 3DVAR analyses of supercells from four real-data cases during spring 2010. For cases in which the WSR-88Ds are located close to the storms, including the 20 April Texas Panhandle and the 10 June Denver tornadic supercells, the 3DVAR analyses contain detailed storm structures, including mesocyclones as indicated by strong midlevel vertical vorticity that were qualitatively verified by reports of either observed tornadoes, large hail, or strong damaging winds. Even for cases in which the WSR-88Ds are located

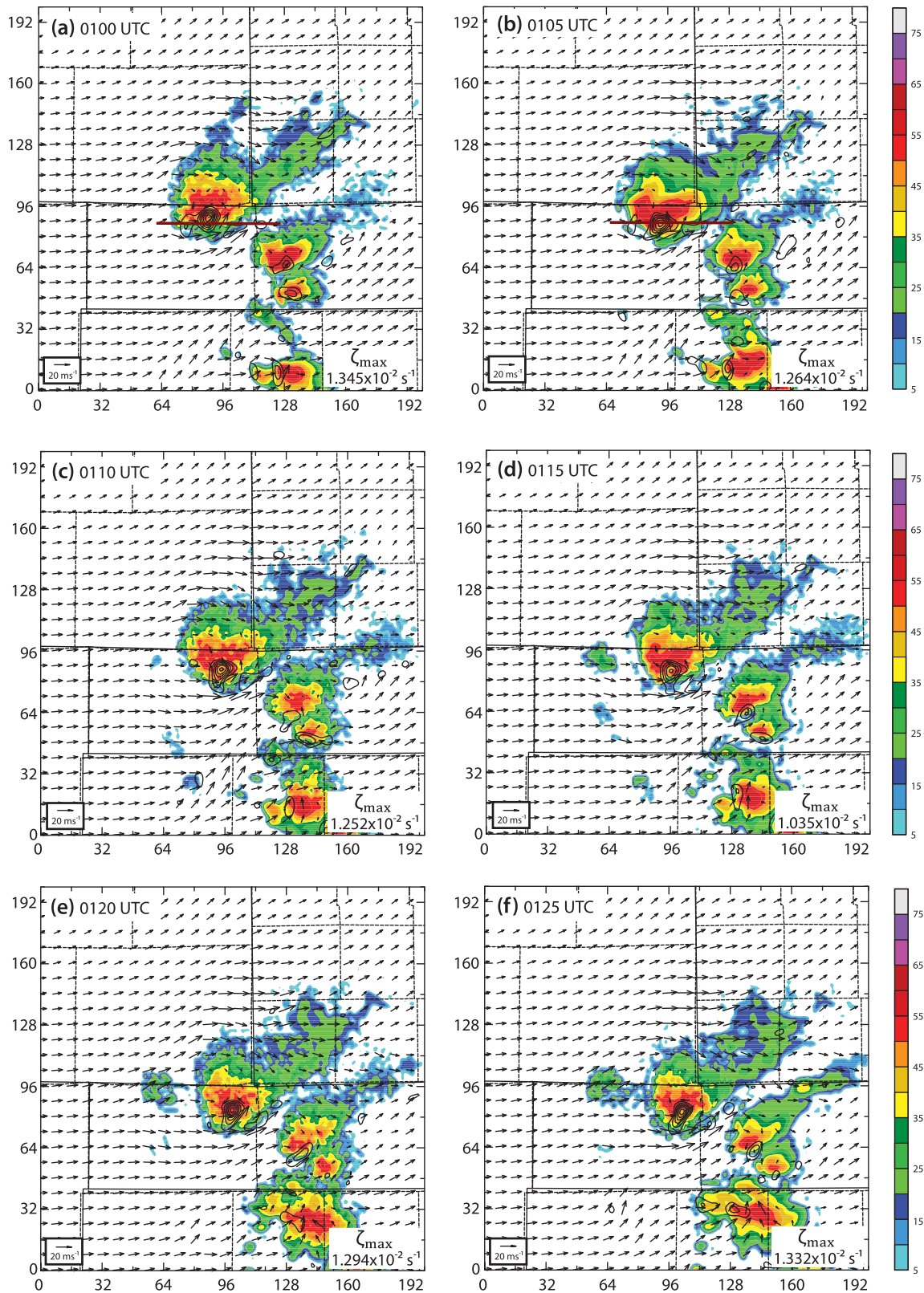


FIG. 10. As in Fig. 4, but for a tornadic supercell event near the boundary of CO and OK using data from radars shown in Fig. 9, at (a) 0100, (b) 0105, (c) 0110, (d) 0115, (e) 0120, and (f) 0125 UTC 1 Jun 2010. Maroon line denotes location of cross sections in Fig. 11.

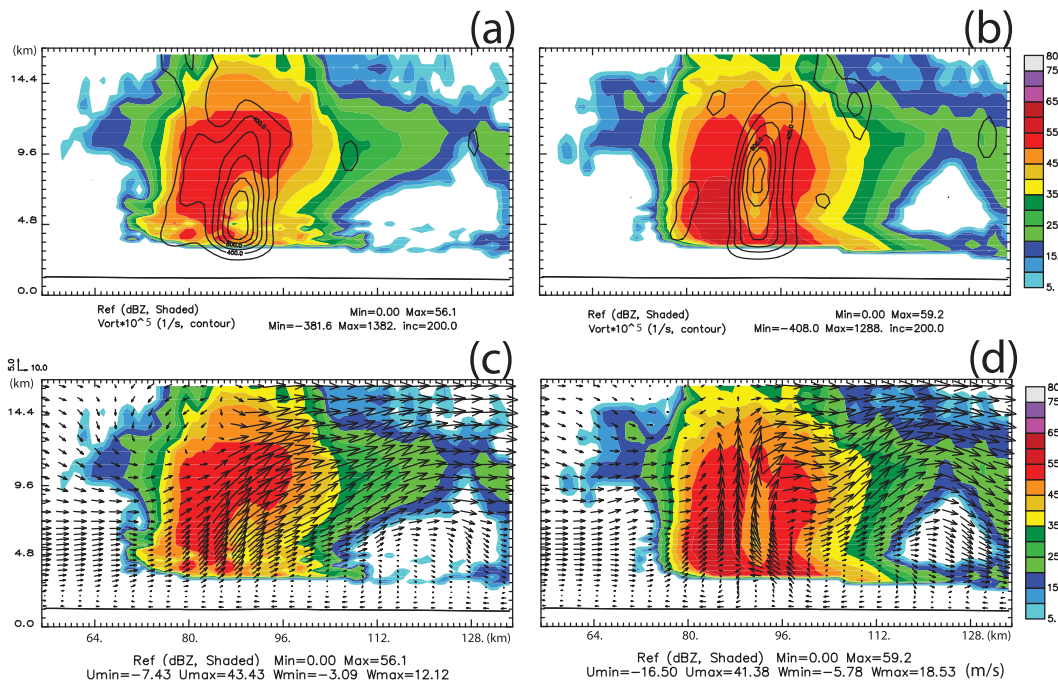


FIG. 11. As in Fig. 5, for a tornadic supercell event near the boundary of CO and OK, valid at (left) 0100 and (right) 0105 UTC 1 Jun 2010.

farther away from the storms, such as the 31 May 2010 Oklahoma panhandle tornadic storm, the middle and upper-level mesocyclones, with associated strong vertical velocity, still can be identified. This study represents the first step in the assessment of this type of analysis approach for use in severe weather warnings. Though we have demonstrated the usefulness of this type of high-resolution analysis with four tornadic thunderstorms, this system cannot resolve tornadoes directly. However, the detection of midlevel mesocyclones can help forecasters increase their confidence in issuing severe weather warnings.

In both the 2011 and 2012 HWT EWP spring experiments, this weather-adaptive 3DVAR system has been improved, and the analyses tested and evaluated by National Weather Service forecasters who participated in HWT EWP program. General positive feedbacks were obtained from the forecasters. For example, one forecaster pointed out that the 3DVAR “highlighted the most intense areas of the storm and provided information on cycling mesocyclones,” while another stated that “it is helpful when the forecaster is sitting on the fence” if there is a need to issue a severe weather warning. More results and feedbacks from

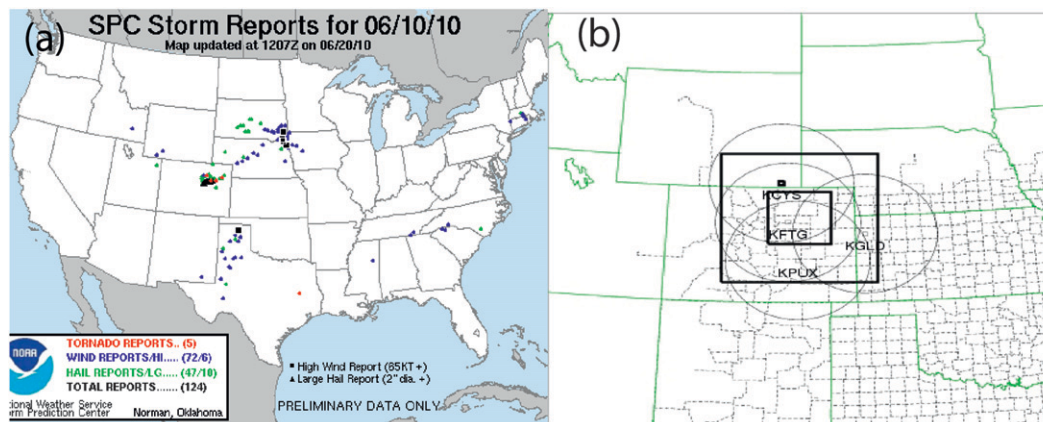


FIG. 12. As in Fig. 3, but for the Denver tornadic storm event on 10 Jun 2010. WSD-88D radars used are KGLD, KFTG, KPUX, and KCYS.

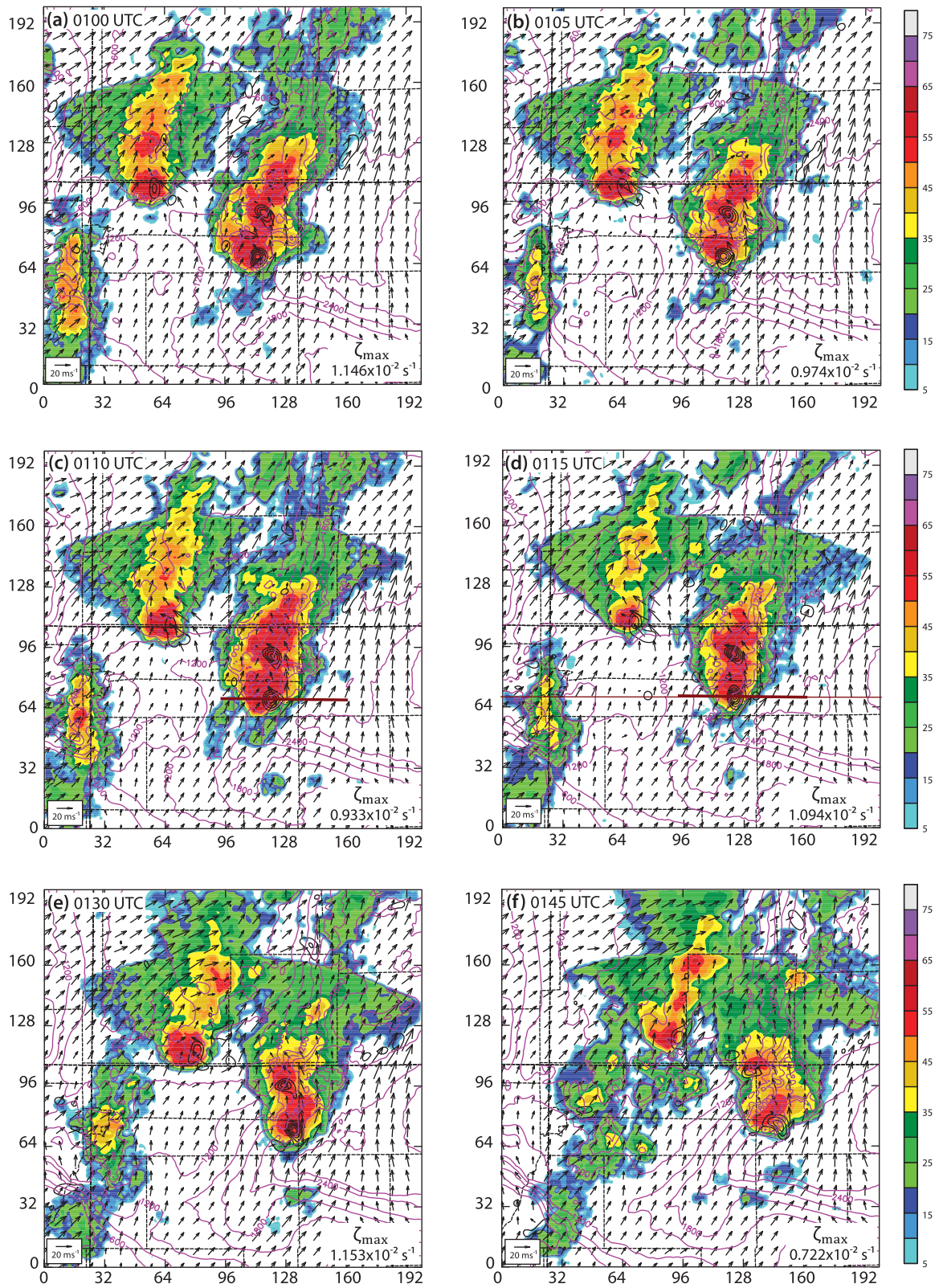


FIG. 13. As in Fig. 4, but for a tornadic supercell event near Denver using data from radars shown in Fig. 12, at (a) 0100, (b) 0105, (c) 0110, (d) 0115, (e) 0130, and (f) 0145 UTC 10 Jun 2010. Purple contours are for CAPE (contour interval is 300 J kg^{-1}). Maroon line denotes location of cross sections in Fig. 14.

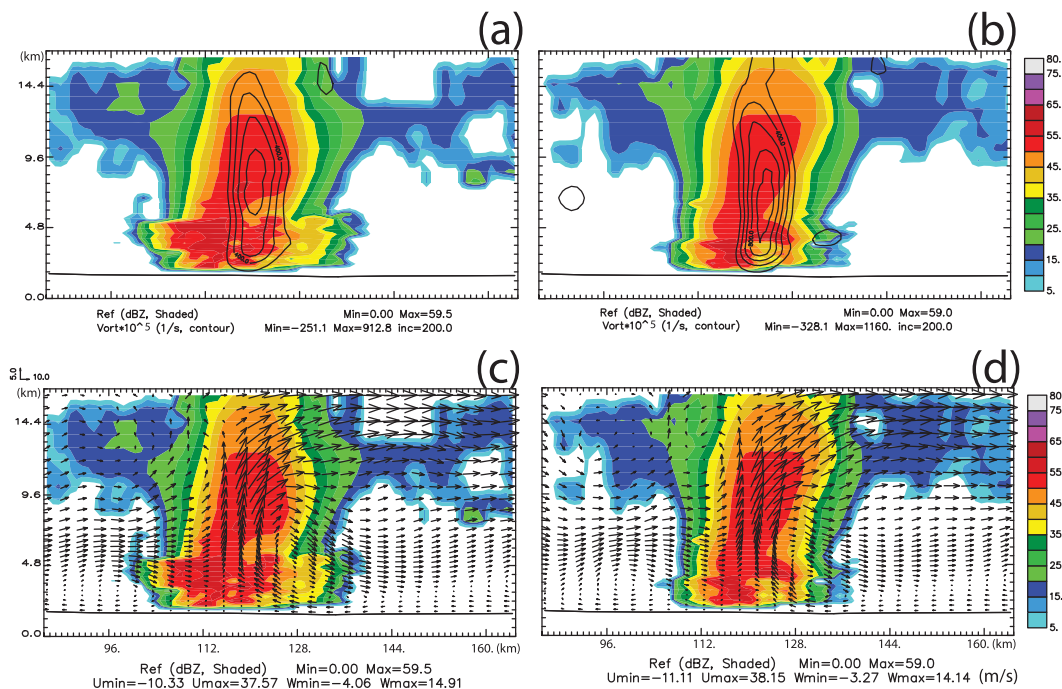


FIG. 14. As in Fig. 5, but for a tornadic supercell event near Denver valid at (left) 0110 and (right) 0115 UTC 10 Jun 2010.

the forecasters will be reported upon in follow-up publications.

Future work includes assimilating additional datasets into this implementation of the 3DVAR system, such as observations from surface mesonets, and the testing of the enhancements to the 3DVAR system to allow for additional equation constraints (e.g., a pressure diagnostic equation) and the direct assimilation of radar reflectivity observations to provide information on hydrometeor types and amounts (Gao and Stensrud 2012). The new system may have greater utility to forecasters than currently available systems. For radar quality control, ongoing work involves incorporating the WDSS-II radar reflectivity quality control (Lakshmanan et al. 2010, 2012), velocity dealiasing (Jing and Wiener 1993), and virtual volume algorithms (Lynn and Lakshmanan 2002) into the 3DVAR radar data preprocessing program.

Acknowledgments. This research was primarily funded by the NOAA Warn-on-Forecast project. The first author was partially supported by NSF Grant ATM-0331756, EEC-0313747, and ATM-0738370 for the earlier ARPS 3DVAR development work done at the Center for Analysis and Prediction of Storms (CAPS). NSF Grants ATM-0331594 and AGS-0802888 also contributed to the development and optimization of the ARPS

3DVAR program. Additional funding was provided by NOAA/Office of Oceanic and Atmospheric Research under NOAA–University of Oklahoma Cooperative Agreement NA08OAR4320904. Chenghao Fu was also supported by the National Basic Research Program of China (Grant 2010CB951904) and National Science Foundation of China (Grant 41075034). We thank Scott Dembek and Jack Kain for their help with optimizing the use of the NSSL computer system. The assistance of Brett Morrow and Steve Fletcher of the NSSL IT team is gratefully acknowledged.

REFERENCES

Barker, D. M., W. Huang, Y.-R. Guo, and Q. N. Xiao, 2004: A three-dimensional (3DVAR) data assimilation system for use with MM5: Implementation and initial results. *Mon. Wea. Rev.*, **132**, 897–914.

Brewster, K., M. Hu, M. Xue, and J. Gao, 2005: Efficient assimilation of radar data at high resolution for short range numerical weather prediction. *World Weather Research Program Symp. and Nowcasting and Very Short-Range Forecasting WSN05*, Toulouse, France, WMO World Weather Research Programme, Symp. CD, Paper 3.06.

—, K. Thomas, J. Gao, J. Brotzge, M. Xue, and Y. Wang, 2010: A nowcasting system using full physics numerical weather prediction initialized with CASA and NEXRAD radar data. Preprints, *25th Conf. Severe Local Storms*, Denver, CO, Amer. Meteor. Soc., 9.4. [Available online at https://ams.confex.com/ams/25SLS/techprogram/paper_176053.htm.]

- Browning, K. A., and R. Wexler, 1968: The determination of kinematic properties of a wind field using Doppler radar. *J. Appl. Meteor.*, **7**, 105–113.
- Bunkers, M. J., M. R. Hjelmfelt, and P. L. Smith, 2006: An observational examination of long-lived supercells. Part I: Characteristics, evolution, and demise. *Wea. Forecasting*, **21**, 673–688.
- , D. R. Clabo, and J. W. Zeitler, 2009: Comments on “Structure and formation mechanism on the 24 May 2000 supercell-like storm developing in a moist environment over the Kanto Plain, Japan.” *Mon. Wea. Rev.*, **137**, 2703–2711.
- Burgess, D. W., 1976: Single Doppler radar vortex recognition: Part I—Mesocyclone signatures. Preprints, *17th Conf. on Radar Meteorology*, Seattle, WA, Amer. Meteor. Soc., 97–103.
- , and L. R. Lemon, 1991: Characteristics of mesocyclones detected during a NEXRAD test. Preprints, *25th Int. Conf. on Radar Meteorology*, Paris, France, Amer. Meteor. Soc., 39–42.
- , and C. A. Doswell III, 1993: Tornadoes and tornadic storms: A review of conceptual models. *The Tornado: Its Structure, Dynamics, Prediction and Hazards, Geophys. Monogr.*, Vol. 79, Amer. Geophys. Union, 161–172.
- , V. T. Wood, and R. A. Brown, 1982: Mesocyclone evolution statistics. Preprints, *12th Conf. on Severe Local Storms*, San Antonio, TX, Amer. Meteor. Soc., 422–424.
- Courtier, P., 1997: Dual formulation of four-dimensional variational assimilation. *Quart. J. Roy. Meteor. Soc.*, **123**, 2449–2461.
- , J.-N. Thépaut, and A. Hollingsworth, 1994: A strategy for operational implementation of 4D-Var, using an incremental approach. *Quart. J. Roy. Meteor. Soc.*, **120**, 1367–1388.
- Daley, R., 1992: *Atmospheric Data Analysis*. Cambridge University Press, 457 pp.
- Doviak, R. J., and D. S. Zrnić, 1993: *Doppler Radar and Weather Observations*. 2nd ed. Academic Press, 562 pp.
- , P. S. Ray, R. G. Strauch, and L. J. Miller, 1976: Error estimation in wind fields derived from dual-Doppler radar measurement. *J. Appl. Meteor.*, **15**, 868–878.
- Droegemeier, K. K., and Coauthors, 2005: Service-oriented environments for dynamically interacting with mesoscale weather. *Comput. Sci. Eng.*, **7**, 12–27.
- Gao, J., and D. Stensrud, 2012: Assimilation of reflectivity data in a convective-scale, cycled 3DVAR framework with hydro-meteor classification. *J. Atmos. Sci.*, **69**, 1054–1065.
- , M. Xue, A. Shapiro, and K. K. Droegemeier, 1999: A variational method for the retrieval of three-dimensional wind fields from dual-Doppler radars. *Mon. Wea. Rev.*, **127**, 2128–2142.
- , —, K. Brewster, F. Carr, and K. K. Droegemeier, 2002: New development of a 3DVAR system for a nonhydrostatic NWP model. Preprints, *15th Conf. on Numerical Weather Prediction/19th Conf. on Weather Analysis and Forecasting*, San Antonio, TX, Amer. Meteor. Soc., 12.4. [Available online at https://ams.confex.com/ams/SLS_WAF_NWP/techprogram/paper_47480.htm.]
- , —, —, and K. K. Droegemeier, 2004: A three-dimensional variational data assimilation method with recursive filter for single-Doppler radar. *J. Atmos. Oceanic Technol.*, **21**, 457–469.
- , D. J. Stensrud, and M. Xue, 2009: Three-dimensional analyses of several thunderstorms observed during VORTEX2 field operations. Preprints, *34th Conf. on Radar Meteorology*, Williamsburg, VA, Amer. Meteor. Soc., P9.8. [Available online at <https://ams.confex.com/ams/34Radar/webprogram/Paper156114.html>.]
- , K. Brewster, M. Xue, J. Brotzge, K. Thomas, and Y. Wang, 2010: Real-time, low-level wind analysis including CASA and WSR-88D radar data using the ARPS 3DVAR. Preprints, *25th Conf. Severe Local Storms*, Denver, CO, Amer. Meteor. Soc., 7B.4. [Available online at <https://ams.confex.com/ams/pdfpapers/176005.pdf>.]
- Ge, G., J. Gao, K. A. Brewster, and M. Xue, 2010: Effects of beam broadening and earth curvature in radar data assimilation. *J. Atmos. Oceanic Technol.*, **27**, 617–636.
- , —, and M. Xue, 2012: Diagnostic pressure equation as a weak constraint in a storm-scale three-dimensional variational radar data assimilation system. *J. Atmos. Oceanic Technol.*, **29**, 1075–1092.
- Gropp, W., E. Lusk, and A. Skjellum, 1999: *Using MPI: Portable Parallel Programming with the Message-Passing Interface*. 2nd ed. The MIT Press, 371 pp.
- Hu, M., M. Xue, and K. Brewster, 2006a: 3DVAR and cloud analysis with WSR-88D level-II data for the prediction of the Fort Worth tornadic thunderstorms. Part I: Cloud analysis and its impact. *Mon. Wea. Rev.*, **134**, 675–698.
- , —, J. Gao, and K. Brewster, 2006b: 3DVAR and cloud analysis with WSR-88D level-II data for the prediction of the Fort Worth, Texas, tornadic thunderstorms. Part II: Impact of radial velocity analysis via 3DVAR. *Mon. Wea. Rev.*, **134**, 699–721.
- Janjić, Z. I., T. L. Black, E. Rogers, H. Chuang, and G. DiMego, 2003: The NCEP nonhydrostatic mesoscale forecasting model. Preprints, *10th Conf. on Mesoscale Processes*, Portland, OR, Amer. Meteor. Soc., 12.1. [Available online at <https://ams.confex.com/ams/pdfpapers/62675.pdf>.]
- Jing, Z., and G. Wiener, 1993: Two-dimensional dealiasing of Doppler velocities. *J. Atmos. Oceanic Technol.*, **10**, 798–808.
- Lakshmanan, V., T. Smith, K. Hondl, G. J. Stumpf, and A. Witt, 2006: A real-time, three-dimensional, rapidly updating, heterogeneous radar merger technique for reflectivity, velocity, and derived products. *Wea. Forecasting*, **21**, 802–823.
- , A. Fritz, T. Smith, K. Hondl, and G. J. Stumpf, 2007a: An automated technique to quality control radar reflectivity data. *J. Appl. Meteor. Climatol.*, **46**, 288–305.
- , T. Smith, G. Stumpf, and K. Hondl, 2007b: The Warning Decision Support System—Integrated Information. *Wea. Forecasting*, **22**, 596–612.
- , J. Zhang, and K. Howard, 2010: A technique to censor biological echoes in radar reflectivity data. *J. Appl. Meteor. Climatol.*, **49**, 435–462.
- , —, K. Hondl, and C. Langston, 2012: A statistical approach to mitigating persistent clutter in radar reflectivity data. *IEEE J. Sel. Top. Appl. Earth Obs. Remote Sens.*, **5**, 652–662.
- Lemon, L. R., and C. A. Doswell III, 1979: Severe thunderstorm evolution and mesocyclone structure as related to tornado genesis. *Mon. Wea. Rev.*, **107**, 1184–1197.
- Liu, D. C., and J. Nocedal, 1989: On the limited-memory BFGS method for large-scale optimization. *Math. Program.*, **45**, 503–528.
- Lorenc, A. C., 1992: Iterative analysis using covariance functions and filters. *Quart. J. Roy. Meteor. Soc.*, **118**, 569–591.
- Lynn, R. J., and V. Lakshmanan, 2002: Virtual radar volumes: Creation, algorithm access, and visualization. Preprints, *21st Conf. on Severe Local Storms*, San Antonio, TX, Amer. Meteor. Soc., 229–232.
- McLaughlin, D., and Coauthors, 2009: Short-wavelength technology and the potential for distributed networks of small radar systems. *Bull. Amer. Meteor. Soc.*, **90**, 1797–1817.

- Miller, L. J., and J. Sun, 2003: Initialization and forecasting of thunderstorms: Specification of radar measurement errors. Preprints, *31st Conf. on Radar Meteorology*, Seattle, WA, Amer. Meteor. Soc., 2B.2. [Available online at https://ams.confex.com/ams/32BC31R5C/techprogram/paper_63885.htm.]
- Purser, R. J., W.-S. Wu, D. Parrish, and N. M. Roberts, 2003: Numerical aspects of the application of recursive filters to variational statistical analysis. Part I: Spatially homogeneous and isotropic Gaussian covariances. *Mon. Wea. Rev.*, **131**, 1524–1535.
- Ray, P. S., and K. K. Wagner, 1976: Multiple Doppler radar observations of storms. *Geophys. Res. Lett.*, **3**, 189–191.
- Schenkman, A., M. Xue, A. Shapiro, K. Brewster, and J. Gao, 2011: The analysis and prediction of the 8–9 May 2007 Oklahoma tornadic mesoscale convective system by assimilating WSR-88D and CASA radar data using 3DVAR. *Mon. Wea. Rev.*, **139**, 224–246.
- Stensrud, D. J., and J. Gao, 2010: Importance of horizontally inhomogeneous environmental initial conditions to ensemble storm-scale radar data assimilation and very short range forecasts. *Mon. Wea. Rev.*, **138**, 1250–1272.
- Stumpf, G. J., A. Witt, E. D. Mitchell, P. L. Spencer, J. T. Johnson, M. D. Eilts, K. W. Thomas, and D. W. Burgess, 1998: The National Severe Storms Laboratory mesocyclone detection algorithm for the WSR-88D. *Wea. Forecasting*, **13**, 304–326.
- Sun, J., and N. A. Crook, 2001: Real-time low-level wind and temperature analysis using single WSR-88D data. *Wea. Forecasting*, **16**, 117–132.
- Xie, Y., S. E. Koch, J. A. McGinley, S. Albers, and N. Wang, 2005: A sequential variational analysis approach for mesoscale data assimilation. Preprints, *21st Conf. on Weather Analysis and Forecasting/17th Conf. on Numerical Weather Prediction*, Washington, DC, Amer. Meteor. Soc., 15B.7. [Available online at <https://ams.confex.com/ams/pdfpapers/93468.pdf>.]
- , —, —, —, P. Bieringer, M. Wolfson, and M. Chan, 2011: A space and time multiscale analysis system: A sequential variational analysis approach. *Mon. Wea. Rev.*, **139**, 1224–1240.
- Xue, M., K. K. Droegemeier, and V. Wong, 2000: The Advanced Regional Prediction System (ARPS)—A multiscale non-hydrostatic atmospheric simulation and prediction model. Part I: Model dynamics and verification. *Meteor. Atmos. Phys.*, **75**, 161–193.
- , and Coauthors, 2001: The Advanced Regional Prediction System (ARPS)—A multiscale nonhydrostatic atmospheric simulation and prediction tool. Part II: Model physics and applications. *Meteor. Atmos. Phys.*, **76**, 134–165.
- , D. Wang, J. Gao, K. Brewster, and K. K. Droegemeier, 2003: The Advanced Regional Prediction System (ARPS), storm-scale numerical weather prediction and data assimilation. *Meteor. Atmos. Phys.*, **76**, 143–165.
- , and Coauthors, 2008: CAPS realtime storm-scale ensemble and high-resolution forecasts as part of the NOAA Hazardous Weather Testbed 2008 Spring Experiment. Preprints, *24th Conf. on Severe Local Storms*, Savannah, GA, Amer. Meteor. Soc., 12.2. [Available online at <https://ams.confex.com/ams/pdfpapers/142036.pdf>.]
- Zhang, F., Y. Weng, J. A. Sippel, Z. Meng, and C. H. Bishop, 2009: Convection-permitting hurricane initialization and prediction through assimilation of Doppler radar observations with an ensemble Kalman filter: Humberto (2007). *Mon. Wea. Rev.*, **137**, 2105–2125.
- Zhang, J., K. Howard, and J. J. Gourley, 2005: Constructing three-dimensional multiple-radar reflectivity mosaics: Examples of convective storms and stratiform rain echoes. *J. Atmos. Oceanic Technol.*, **22**, 30–42.
- , and Coauthors, 2011: National Mosaic and Multi-sensor QPE (NMQ) system: Description, results, and future plans. *Bull. Amer. Meteor. Soc.*, **92**, 1321–1338.
- Zhao, K., X. Li, M. Xue, B. J.-D. Jou, and W.-C. Lee, 2012: Short-term forecasting through intermittent assimilation of data from Taiwan and mainland China coastal radars for Typhoon Meranti (2010) at landfall. *J. Geophys. Res.*, **117**, D06108, doi:10.1029/2011JD017109.